actuators

MDPI

Article

Novel Design and Modeling of a Soft Pneumatic Actuator Based on Antagonism Mechanism

Yinglong Chen, Junhao Zhang and Yongjun Gong *

Naval Architecture and Ocean Engineering College, Dalian Maritime University, Dalian 116026, China; chenyinglong@dlmu.edu.cn (Y.C.); dmuzjh@163.com (J.Z.)

* Correspondence: yongjungong@163.com

Received: 22 September 2020; Accepted: 13 October 2020; Published: 21 October 2020

Abstract: The soft actuator possesses the characteristics of flexibility, environmental adaptability, and human–machine interaction. Firstly, aiming to resolve the limitation of variable stiffness performance of a traditional pneumatic artificial muscle (PAM) actuator, based on the antagonistic mechanism of extensor and contractor muscles, a novel pneumatic soft actuator coupled of extensor and contractor muscles is proposed in this paper. The actuator can perform the compound action of elongation/contraction, and the stiffness of it can be controlled by adjusting the elongation and contraction forces. Secondly, based on the deformation principle of woven and elastic fabric layers, the mechanical characteristics model of the actuator is established and simulated. The mechanical properties of the actuator are tested under different pressures and deformation displacement and the variable stiffness characteristics of the actuator are verified. Finally, actuators are utilized to manufacture a soft mechanical manipulator, which can achieve variable stiffness in a fixed bending attitude.

Keywords: soft actuator; extensor; contractor; antagonism

1. Introduction

Soft actuators are made of flexible materials or a few added rigid materials, and have the advantages of high flexibility and adaptability to complex environments. In recent years, they have attracted extensive attention from institutions and scholars, that have made significant progress, such as the pneumatic artificial muscle made of elastic rubber and fabric [1], octopus-like tentacle robotics driven by shape memory alloy [2], and an artificial muscle driven by electroactive polymer [3].

In practical applications, soft actuators need not only excellent flexibility, but also a stable and controllable body shape and output force under certain conditions. Therefore, the soft actuator with variable stiffness has extremely high research significance. In previous research, there are two main principles for the variable stiffness of soft actuators. The first principle is to add antagonism to the material to keep the mechanism stable, such as: coupling structure [4,5], layer interference structure [6], and blocking principle [7]. The second principle is to obtain variable stiffness through the phase change between the solid and liquid forms of the material, such as magnetic fluid [8]. A common feature of these variable stiffness principles is the dependence on elastomeric materials, such as urethane and silicon, for the soft actuator body. These materials possess many superiorities, including corrosion and heat resistance, the ability to co-mold multiple materials, and the ability to withstand large deformations when performing complex ranges of motion.

However, these superiorities are not unique to elastomeric materials. Fabrics also provide a wide range of stretch properties, when strategically utilized, they can produce appropriately deformation desired in the design of soft actuators.

In this paper, based on the antagonistic mechanism of soft extensor and contractor muscles, a soft actuator with a coupled driving structure is designed and fabricated. The coupling structure achieves variable stiffness by forming an antagonism between the structures. The representative actuator is octopus-like tentacle structure [4,9], adopts the method of "transverse muscle" and "longitudinal muscle" to tighten the structure, achieving variable stiffness. However, it cannot perform the independently control of stiffness and position. The soft actuator proposed in this paper can perfectly solve this problem.

We provide detailed design and manufacturing methods to explain how to construct soft actuators from woven and elastic fabric products commonly found in clothing. Specifically, we show that the extensor and contractor muscles reinforced by these two fabrics are coupled together internally and externally, making the soft actuator variable stiffness. Moreover, based on the principle of virtual work, the mechanical characteristic model and corresponding stiffness model of the soft actuator are established, and the simulation analysis is carried out. Finally, the mechanical characteristics of the actuator are tested, and the pressure of the extensor and contractor muscles are controlled to adjust the variable stiffness characteristics. In addition, we demonstrate the utility of the proposed actuators by integrating them into a soft manipulator that is capable of varying stiffness while keeping a fixed bending attitude.

2. Design and Fabrication

In this section, we detail the design inspiration and thoughts of the proposed actuator. Moreover, discussions on fabrication process including steps and consideration are presented.

2.1. Design

Based on the previous research [10–17], there are limitations associated with traditional soft actuator. These limitations are summarized as follows:

- The pneumatic artificial muscle only generates a contraction force when pressurizing.
- The extensor actuator only generates extension force when pressurizing.
- Each soft actuator type has an invariable stiffness at a specific length.

In view of the limitations in the above research, our design of the soft actuator is based on starfish, because starfish consists of special features, including connective tissue, calcite bone and interosseous muscle [18], which allows it to actively regulate the structural stiffness of its body. Since the movement of the elastic body of the actuator depends on the deformation of the fabric, especially the characteristics of the material used in its construction, this article combines two anisotropic fabrics (woven fabric and elastic fabric) and elastomer (silica gel) to design contractor and extensor respectively. Finally, the two are compounded into the inner and outer chamber structure and defined as the extensor-contractor fabric-based antagonistic actuator (ECFA). When the two chambers are controlled with different pressures, variable stiffness of the actuator can be achieved.

The overall design of the actuator is shown in Figure 1c. There are numerous design factors that determine the parameter of the actuator, such as the lateral structure, cross section, and so on. The actuator is cylindrical in shape and has two holes, which are used to pressurize the extensor and contractor respectively, P_{con} is used to inflate contractor and P_{ex} is used to inflate extensor. The two ends of the actuator are sealed and fixed by compressing rings. The outer layer of extensor and contractor is wrapped in two different functional fabrics. For the bladder body (green and yellow parts in Figure 1c), it should have better tensile and strength properties to ensure that it can be stretched or contracted during the pressurization process and will not be damaged by air pressure. Silica gel has natural flexibility and strength, which is the best choice for the bladder body. However, after the casting of silica gel body, if there is no restriction on the outer layer, the extensor will only expand radially and not extend after being pressurized, because the side wall area of the bladder body is larger than top wall area. In order to solve this problem, many scholars used the double helix fibers to wrap around the

outer layer of the bladder body [19], which can improve the input pressure, but there is a gap between the double helix fibers, and there is irregular expansion. In this paper, fabrics as the reinforcement layer can effectively limit the expansion of the extensor and improve the elongation efficiency.

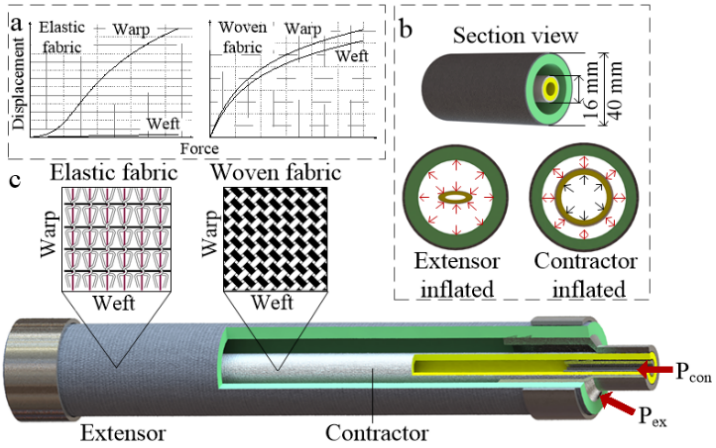

Figure 1. A conceptual representation of the soft actuator. (**a**) Force-deformation test of fabrics in warp and weft direction. (**b**) Section view of the actuator and state of extensor and contractor bladders in inflation. (**c**) Overall structure of actuator.

The fabric chosen for the extensor muscle should have maximum strain under load. Elastic fabrics are highly suitable for this layer because their structures enable maximal mechanical compliance in axial direction and stretches performance poorly in the radial direction. We chose a plain warp-knitted latex-polyester textile (warp direction is high elasticity latex yarn, weft direction is low elasticity polyester) for its low elastic modulus, low weight, and sewability properties. We experimentally tested the force-displacement characteristics of specimens of the selected elastic fabric and render the results in Figure 1a (left part) (warp and weft directions). For the inner layer, we want a textile with bidirectional strain (in this case longitudinal) and a certain basic stretch. We chose a commercially plain weave polyamide textile, for its bidirectional stretch, stability, and durability. Woven fabrics can exhibit more pronounced isotropic behavior than elastic fabric counterparts because their diamond shaped construction creates inherent structural deformation that can be exploited along with the choice of nylon material. In addition, woven fabrics are generally balanced, meaning their structures are characterized by symmetry. The results of force-displacement test on the selected woven fabrics are reported in Figure 1a (right part).

When the value of P_{ex} is larger, the actuator will elongate and produce extension force, simultaneously, the contractor will be flattened, as shown in Figure 1b (bottom left). When the value of P_{con} is larger, the actuator will be shortened, and the contractor inside will expand, as shown in Figure 1b (bottom right). The contraction force of contractor has an antagonistic relationship with the elongation force of extensor, so we can coordinate the two forces to achieve stiffness control. During this process, it is necessary to make sure that the outer diameter of the expanded contractor is smaller than the inner diameter of the extensor. According to the above design principles, the size of the actuator designed is established.

2.2. Fabrication

The manufacture process of the actuator is fabricated in four stages. In the first stage, as shown in Figure 2a, a core defines the hollow geometry of the bladder body and a mold defines the exterior geometry, the two are assembled by four screws. The gap between mold and core is sealed with raw tape. Three-dimensional printing of the molds enables rapid iteration of cross-sectional geometry, actuator length, and enables features such as thread winding paths to be molded into the exterior surface of the bladders. The second stage after the completion of mold preparation stage is the silica gel

modulation stage. The bladders of extensor and contractor are made of silica gel (ELASTOSIL® M4601 A/B, the mixing ratio is 9:1, performance parameters at 23 °C are shown in Table 1). Component B contains platinum catalyst to improve the solidification rate of component A. Mixed silica gel was put into a centrifugal mixer for full mixing, and then put into the vacuum generator to remove bubbles. Then slowly pour the silica gel into the mold to prevent small bubbles. After baking and curing, the extensor capsule is completed, as shown in Figure 3b, and the outer surface is slotted to wind the filaments. The manufacturing process of extensor and contractor bladders is the same, but the size of the mold and core is different. Moreover, there are no grooves on the outer surface of the contractor bladder. In the third stage (Figure 2c), for enhancing the strength of the bladders, a strain limiting fibers (aramid 1414) applied to the outer surface of extensor bladder, which also in order to limit its expansion. Then, the bladder is fabricated by cutting the elastic fabric layer and sewing them together along two edges using a flat overlock sewing machine to form a cylinder. The contractor does not entangle strain limiting fibers, and the woven fabric layer used is naturally cylindrical, so the bladder can be directly inserted into the woven fabric. The fourth stage involves inserting the endcaps into the two ends of the extensor and contractor, subsequently inserting the already assembled contractor into the extensor, before the joints between the endcaps are fixed and sealed with glue (Figure 2d). Then, clamping the two ends of the outer surface of extensor with two iron hoops (Figure 2e) improves the tightness of the actuator. Finally, we optimized the shape and size of the endcaps, and the finished physical body is shown in Figure 2f.

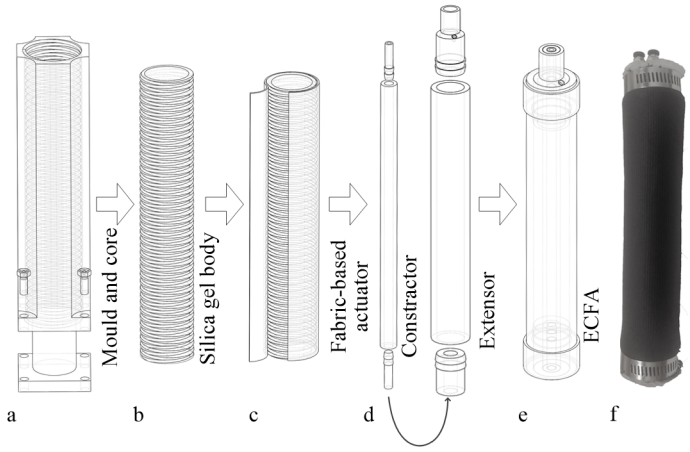

Figure 2. Schematic diagram outlining stages of the actuator fabrication process. (**a**) In the first molding step, the actuator is molded using 3D printed mold and core. (**b**) The bladders are obtained by demolding, and fiber reinforcing thread is wound along the length of the bladders. (**c**)Then the anisotropic fabrics are wrapped on the bladders, and the junction is sewn to obtain the fabric-based actuator. (**d**) Insert the connector into the two ends of the extensor and the contractor, then insert the contractor into the extensor, seal and connect the junction is with glue. (**e**) Clamp two ends of the actuator with two rings. (**f**) Physical body of the soft actuator.

Table 1. Performance index of silica gel at 23 °C.

Property	Unit	Value
Viscosity	[mPa s]	20.000
Density	[g/cm^3]	1.13
Tensile Strength	[N/mm^2]	6.5
Tear Strength	[N/mm]	30
Linear Shrinkage	[%]	0.1

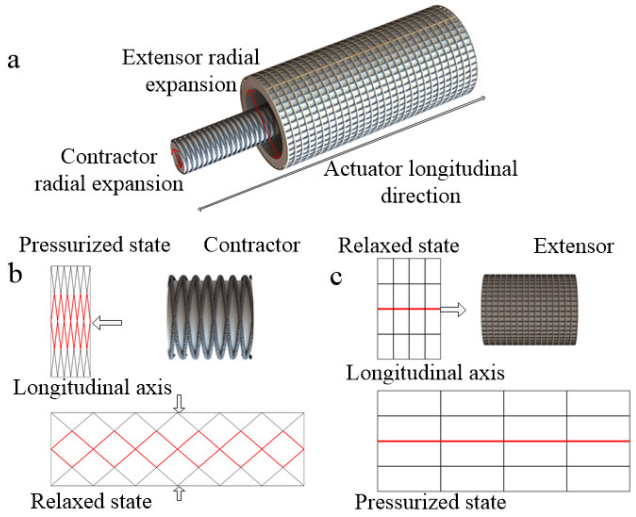

Figure 3. Mathematical model analysis. (**a**) Simplified model diagram of actuator. (**b**) The movement of the woven fabric when the extensor pressurized firstly and contractor is pressurized lately. (**c**) The movement of the elastic fabric when the extensor is pressurized.

3. Mathematical Model

The output force mathematical model is derived based on the principle of virtual work. First of all, we simplify the structure and fabric layers of soft actuator as shown in Figure 3a. The contractor can be considered as a PAM, which fabric layer can be cut across a line parallel to the longitudinal axis (red line in Figure 3b) and then folded flat shape. The flat fabric behaves like a subdivision of a scissor mechanism, which can expand along its width while shrinking along its length. This movement corresponds to the radial expansion and longitudinal contraction of contractor muscle. In the absence of the braided layer, the motion is governed solely by the mechanics of the bladder material. The fabric layer of extensor can be seen as a cross structure of warp and weft, because weft yarn is low-elastic polyester, it will hardly deform, and warp yarn is latex yarn, which has excellent deformation performance. Additionally, it can be seen from reference [20] that the yarns bound to the warp yarn are not the main force bearing body. When the extensor is elongated by pressurization, the change in the yarn of the fabric layer is shown in Figure 3c. To sum up, contractor muscle relies on the structural deformation, and extensor muscle relies on the material deformation. The extensor and contractor muscle perform different movements, which causes the actuator to output different force.

Figure 4 illustrates the geometry parameter of the actuator, including contractor and extensor, assuming the actuator is perfectly cylindrical and the length l, diameter d, and θ represent the braid angle between a single braided thread and the actuator central axis. The single thread of the fiber b encircles the contractor n times. p_1 is pressure inside contractor and p_2 is the extensor pressure.

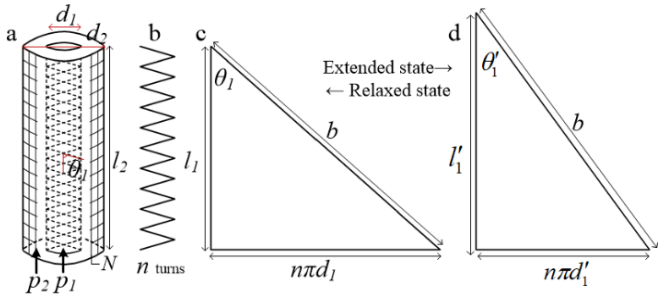

Figure 4. Parameter drawings of the soft actuator concept. (**a**) Geometry parameter of actuator. (**b**) A single-turn yarn of woven fabric outer the contractor muscle. A right triangle formed by the length of a single-turn yarn as a hypotenuse, (**c**) is under relaxed state and (**d**) is extended state.

When different pressures are applied to the extensor and contractor, the soft actuator will extend or contract motion, and at the same time will output force, that is, the output force of the actuator is the result of the joint action of the extensor and contractor. The output force of the actuator F_{total} can be written as:

$$F_{\text{total}} = (F_{\text{contractor}} - F_{\text{extensor}}) \begin{cases} if\ F_{\text{total}} > 0 \rightarrow contraction\ force \\ if F_{\text{total}} < 0 \rightarrow extension\ force \end{cases} \quad (1)$$

where $F_{\text{contractor}}$ is contractor force and F_{extensor} is extensor force.

The contractor muscle is mainly composed of silicone body and woven fabric layer. Its output force is the vector sum of the elastic force of the silicone body and the friction between the fabric layer and silicone body. The contractor output force $F_{\text{contractor}}$ can be written as:

$$F_{\text{contractor}} = F_{1\text{ideal}} - F_{1\text{friction}} - F_{1\text{elastic}} \quad (2)$$

where $F_{1\text{ideal}}$ is the ideal output force of the contractor, $F_{1\text{friction}}$ is the friction between the fabric layer and silicone body, and $F_{1\text{elastic}}$ is elastic force of the silicone body.

The ideal output force of contractor $F_{1\text{ideal}}$ can be derived from the following formula.

Firstly, based on the work of Chou and Hannaford [21], a common ideal model is proposed based on the principle of virtual work as follow:

$$F = -P' \frac{dV}{dL} \quad (3)$$

where P' is working pressure. V and L is the volume and length in the current state respectively.

For contractor muscle, the working pressure is affected by the pressure inside the extensor, for example, a higher pressure in the extensor reduces the relative pressure in the contractor. So it's working pressure P'_1 can be written as:

$$P'_1 = P_1 - P_2 \quad (4)$$

and relaxed volume V_1 can be written as:

$$V_1 = \frac{\pi d_1^2 l_1}{4} \quad (5)$$

where V_1, l_1, and d_1 are the volume, length, and diameter of contractor in the relaxed state, respectively.

According to the geometric structure of the woven fabric, the following relationship is obtained:

$$\frac{d_1}{d'_1} = \frac{\sin\theta_1}{\sin\theta'_1} \quad \frac{l_1}{l'_1} = \frac{\cos\theta_1}{\cos\theta'_1} = 1 + \varepsilon \quad (6)$$

where θ_1 is the braid angle in the relaxed state, d'_1, θ'_1, and l'_1 are diameter, braid angle and length in the pressurized state. ε is elongation rate of the actuator.

Substituting Equations (4)–(6) into Equation (3), the ideal output force of contractor $F_{1\text{ideal}}$ can be obtained:

$$F_{1\text{ideal}} = (\pi d_1^2/4)(p_1 - p_2)[\frac{3(1+\varepsilon)^2}{\tan^2\theta_1} - \frac{1}{\sin^2\theta_1}] \quad (7)$$

The friction $F_{1\text{friction}}$ between the fabric layer and silicone body can be derived from the following formula.

According to the movement of the contractor, the silicone body is closely attached to the woven fabric layer during the contraction process, and the internal pressure is completely transmitted to the woven fabric layer. The friction coefficient between the fabric layer and the silicone body is much

larger than that between the fiber strands, and the strands slide against each other, so that only the friction force between the fabric layer and the silicone body is considered, the expression of $F_{1\text{friction}}$ is:

$$F_{1\text{friction}} = f_s S_{1\text{contact}} P'_1 \tag{8}$$

where f_s is friction coefficient and $S_{1\text{contact}}$ is the contact area of the fabric layer and the silicone body at any braid angle.

Assuming that the fabric layer completely covers the internal silicone body when it is stretched (pressurized), and there is no mesh between the multiple flat yarns, its physical structure is shown in Figure 5e and the schematic is shown in Figure 5f. The axis line is the length of the actuator direction. According to the geometry in different states, the contact area of the fabric layer at any braid angle can be obtained.

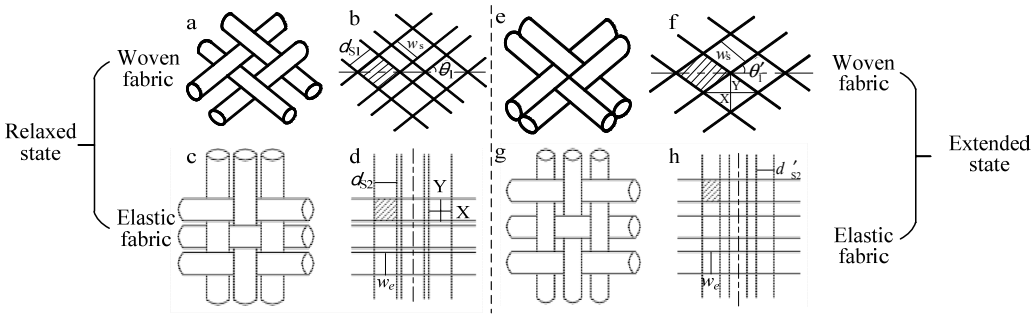

Figure 5. Shape of the fabric layers in different states. (**a**) Woven fabric in relaxed state and (**b**) is schematic. (**c**,**d**) Elastic fabric in relaxed state. (**e**,**f**) Woven fabric in extended state. (**g**,**h**) Elastic fabric in extended state.

According to the area formula of the diamond, the area of a single mesh d'_S in the extended state can be calculated as:

$$d'_S = W_S^2 / 2\cos\theta'_1 \sin\theta'_1 \tag{9}$$

where $W_S = S_1 d_{S1}$ is the bundle width composed of S_1 parallel yarns, and d_{S1} is the diameter of a single yarn. Thus, the total number of contact surface mesh N_S is:

$$N_S = \frac{\pi d_1 l_1}{d'_S} = \frac{2\pi d_1 l_1 \cos\theta'_1 \sin\theta'_1}{S_1^2 d_{S1}^2} \tag{10}$$

In the relaxed state, the physical structure is shown in Figure 5a and the schematic is shown in Figure 5b. The area of a single mesh d_S is $d_S = \boldsymbol{W_S^2}/2\cos\theta_1\sin\theta_1$, so the contact area of the fabric layer and silicone body at any braid angle can be obtained:

$$S_{1\text{contact}} = N_S d_S = \frac{\pi d_1 l_1 \sin\theta_1}{(1+\varepsilon)\sqrt{1-\cos^2\theta_1(1+\varepsilon)^2}} \tag{11}$$

The elastic force of the silicone body $F_{1\text{elastic}}$ is:

$$F_{1\text{elastic}} = \varepsilon E_R l_1 \tag{12}$$

where E_R is the elastic modulus of the silicone body.

In summary, the output force of the contractor $F_{\text{contractor}}$ can be obtained.

Similarly, the extensor muscle is mainly composed of silicone body and elastic fabric layer. Its output force is the vector sum of the elastic force of the silicone body and the friction between the elastic fabric layer and silicone body. The extensor output force F_{extensor} can be written as:

$$F_{\text{extensor}} = F_{2\text{ideal}} - F_{2\text{friction}} - F_{2\text{elastic}} \tag{13}$$

where $F_{2\text{ideal}}$ is the ideal output force of extensor, $F_{2\text{friction}}$ is the friction between the elastic fabric layer and silicone body, and $F_{2\text{elastic}}$ is the elastic force of the silicone body.

The ideal output force of extensor $F_{2\text{ideal}}$ can be derived from the following formula.

The extensor muscle is affected by the volume of the contractor muscle. In fact, the contractor muscle represents a hollow cylindrical portion along the center of the extensor muscle. This means the actual shape of the extensor muscle is represented by a thick wall cylindrical shell, so the working pressure of extensor P_2' is:

$$P_2' = P_2 \tag{14}$$

In the relaxed state, the length of the extensor muscle is equal to that of the contractor muscle, and the diameter is 2.5 times that of the contractor muscle, that is:

$$l_2 = l_1 \;\; d_2 = 2.5d_1 \;\; V_2 = 6.25V_1 \tag{15}$$

where l_2, d_2, and V_2 are the length, diameter, and volume of extensor.

Substituting Equations (14) and (15) into Equation (3), the ideal output force of extensor $F_{2\text{ideal}}$ can be obtained:

$$\begin{aligned} F_{2\text{ideal}} &= p_2 \tfrac{dV_r}{dl_2} = p_2\left(\tfrac{dV_2}{dl_2} - \tfrac{dV_1}{dl_1}\right) \\ &= \tfrac{5.25}{4}\pi d_1^2 p_2\left[\tfrac{3(1+\varepsilon)^2}{\tan^2\theta_1} - \tfrac{1}{\sin^2\theta_1}\right] \end{aligned} \tag{16}$$

where V_r is the effective volume of the cylinder representing the extensor.

The friction force between the elastic fabric layer and the silicone body $F_{2\text{friction}}$ is:

$$F_{2\text{friction}} = f_\text{E} S_{2\text{contact}} P_2' \tag{17}$$

where f_E is friction coefficient and $S_{2\text{contact}}$ is the contact area of the elastic fabric layer and the silicone body.

Different from contractor muscle that assuming that the fabric layer completely covers the internal silicone body when it is relaxed (unpressurized), its physical structure is shown in Figure 5c and the schematic is shown in Figure 5d. The axis line is the length direction of the actuator, correspondingly, the warp direction of the elastic fabric is the latex yarn. When the extensor is pressurized, the latex yarn will be stretched, and the diameter will become slightly smaller. At the same time, the gap between the warp and weft yarns of the elastic fabric will become larger, as shown in Figure 5g,h.

In the relaxed state, the area of a single mesh d_E is:

$$d_\text{E} = W_E N d_{E2}^3 \tag{18}$$

where $W_\text{E} = S_2 d_{\text{E2}}$ is the bundle width composed of S_2 parallel latex yarns, and d_{E2} is the diameter of a single latex yarn. N is the number of bundles.

Thus, the total number of mesh N_E is:

$$N_\text{E} = \frac{\pi d_2 l_2}{d_E} = \frac{\pi d_2 l_2}{S_2 N d_{E2}^4} \tag{19}$$

In the extended state, the area of a single mesh $d_E^{'}$ is:

$$d_E^{'} = S_2 d_{E2}^2 d_{E2}'^2 \tag{20}$$

where d'_{E2} is the diameter of the latex yarn is stretched in the extended state, and $d'_{E2} \approx \varepsilon d_{\mathrm{E2}}$.

So, the contact area of the elastic fabric layer and silicone body can be obtained:

$$S_{2\mathrm{contact}} = N_E d'_E = \frac{\pi d_2 l_2}{N} \frac{d'^2_{E2}}{d^2_{E2}} = \frac{\pi d_2 l_2 \varepsilon^2}{N} \tag{21}$$

The silicone body of the extensor and contractor muscles are the same material, so the elastic force of the silicone body $F_{2\mathrm{elastic}}$ of extensor is:

$$F_{2\mathrm{elastic}} = \varepsilon E_R l_2 \tag{22}$$

Therefore, the output force of the extensor F_{extensor} can be obtained.

In summary, the total output force of the actuator F_{total} is:

$$F_{\mathrm{total}} = \pi d_1 l_1 \left[\frac{3 f_E (P_1 - P_2)\varepsilon^2}{N} - \frac{f_S P_2 \sin\theta_1}{(1+\varepsilon)\sqrt{1-\cos^2\theta_1 (1+\varepsilon)^2}}\right] - \frac{\pi d_1^2}{4}(6.25 p_2 - p_1)\left[\frac{3(1+\varepsilon)^2}{\tan^2\theta_1} - \frac{1}{\sin^2\theta_1}\right] \tag{23}$$

This output force model is suitable for that considering friction, soft actuators with internal and external muscle composite structures, and the output force can be predicted based on the input pressure and posture accurately. Compared to previous studies on soft actuators [22,23], they did not take friction into account.

The values of constants and variables in the above formula are shown in Table 2, where includes the elongation rate that can be reached by passive control. For example, the actuator itself can only reach a contraction rate of −0.05 through pressurizing. On the basis of a 10-mm contraction of the actuator, we control the *z*-axis stepping motor of the three-degree-of-freedom platform which moves down 10 mm again to make the actuator in a compressed state, so that the shrinkage rate can reach −0.1. The elongation rate change range we use in the simulation and experiment is −0.1~0.2.

Table 2. Parameter of the soft actuator.

Parameter	Description	Value
d_1	Diameter of contractor	16 mm
l_1	Length of contractor	200 mm
θ_1	Braid angle in the relaxed state	45.2°
f_{S}	Friction coefficient of woven fabric	0.005
f_{E}	Friction coefficient of elastic fabric	0.25
p_1	Input pressure of contractor	0~0.3 MPa
p_2	Input pressure of extensor	0~0.3 MPa
ε	elongation rate	−0.1~0.2
N	bundles of latex yarns	60

Next we discuss the static stiffness model of the soft actuator. The output force of the actuator is a function of input pressure and length, and the static stiffness model is the derivative of the output force with respect to length. So, the static stiffness of the actuator K_{actuator} can be expressed:

$$K_{\mathrm{actuator}} = \frac{dF_{\mathrm{total}}(\varepsilon)}{\mathrm{d}l} \tag{24}$$

Substituting Equation (23) into Equation (24), the static stiffness K_{actuator} can be obtained:

$$\begin{aligned} K_{\text{actuator}} &= \frac{3\pi d_1 l_1 f_E}{N}\frac{d\varepsilon^2}{dl} \\ &-\pi d_1 l_1 f_S \sin\theta_1 \frac{d[1/(1+\varepsilon)\sqrt{1-\cos^2\theta_1(1+\varepsilon)^2}]}{dl} \\ &-\frac{3\pi d_1^2(6.25p_2-p_1)}{4\tan^2\theta_1}\frac{d(1+\varepsilon)^2}{dl} \end{aligned} \tag{25}$$

where the second polynomial is excessively complicated and, after simplification, is approximately $\pi d_1 l_1 f_s/(1+\varepsilon)$, then merging with the first polynomial, the last is about 0. So:

$$K_{\text{actuator}} = (6.25p_2 - p_1)\frac{3\pi d_1^2(1+\varepsilon)}{2l_1\tan^2\theta_1} \tag{26}$$

It can be found from the above formula that the stiffness of the soft actuator is also related to the input pressure of the extensor and contractor, and the influence ratio of the extensor is larger because the volume of its chamber is larger. It is also related to the overall elongation rate, which is controllable, on the one hand, it can be automatically extended by pressurizing, on the other hand, it can be artificially intervened to apply additional contraction or extension force, which will all affect the stiffness of the actuator.

4. Experimental Verification

In this section, we detail static force experimental verification. In addition, we test the tensile stiffness of the proposed soft actuator and the tensile stiffness can achieve variable stiffness at a fixed length. Also, we tested the bending stiffness under corresponding pressure.

4.1. Static Force Analysis

Figure 6a shows the experimental system for testing the ECFA including electrical and pneumatic circuit diagrams, the physical diagram can be seen in Figure 6b, which mainly contains a microcontroller (Arduino Mega 2560) and two proportional pressure reducing valves. The computer is connected to the microcontroller via USB and provides power to it. The microcontroller outputs a PWM (pulse width modulation) signal. The PWM signal is converted into a voltage signal by the "PWM to voltage" module. This module is powered by 12 V voltage, and then the voltage signal is sent to the valves. In this process, the output pressure of the valves port is changed by controlling the movement of the proportional solenoid. Valve ① supplies pressure to the contractor and valve ② supplies pressure to the extensor. The entire pneumatic circuit is provided with a source by an air compressor, and filtered and decompressed by a pneumatic couplet (an air filter and a pressure reducing valve).

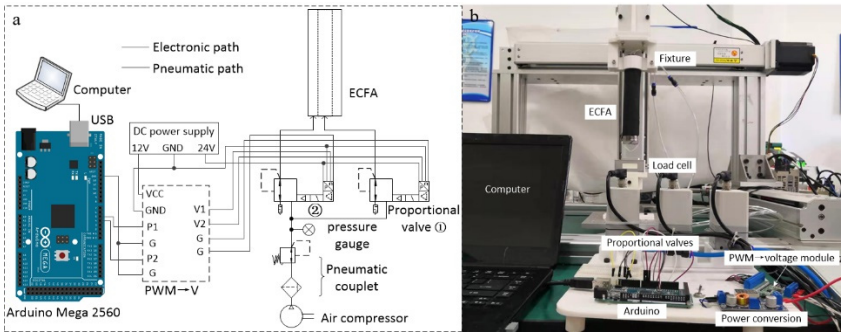

Figure 6. Experiment setup. (**a**) Schematic diagram of electronic path and pneumatic path. (**b**) Physical diagram.

The experimental setup shown in Figure 7a is experimental verification for output force of ECFA. A 3D printed fixture is used to suspend the ECFA vertically in the air and the fixture is fixed on a

three-degree-of-freedom test platform. The platform mainly includes three stepping motors, three sets of ball screws and a sliding table module, which can conveniently adjust the spatial position of the actuator. When testing its output force, the free end of the ECFA is connected to the second fixed point of a load cell by adjusting the position of a ball screw, and the load cell is also fixed on the 3D printed fixture. However, there is no restraint object around the ECFA when pressurizing, it will produce buckling or lateral deformation, as shown in Figure 7b. To solve this problem, we design a corresponding bracket (see Figure 7c) to restrain the deformation of ECFA, and the bucket is fixed on the load cell. The diameter of the bracket is slightly larger than the diameter of the ECFA, which can effectively improve the accuracy and reliability of the measurement, and will not affect the output force.

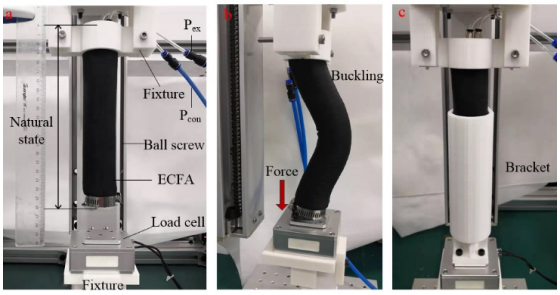

Figure 7. Test the output force of ECFA. (**a**) Calculating the force of the ECFA. (**b**) Buckling of the ECFM when was pressurized. (**c**) calculating the extension force of the ECFA with a 3D-printed rigid bracket.

We tested the pressure-displacement characteristics of ECFA. When the extensor and contractor muscles were pressurized separately, displacement in the opposite direction would occur, as shown in Figure 8a. Therefore, we can actively control the actuator's movement range from −0.05 to 0.18. The positive displacement caused by the extensor is larger because the resistance of the contractor is smaller and the action area of pressure is larger. From this, it can be seen that the reverse displacement caused by the contractor is smaller.

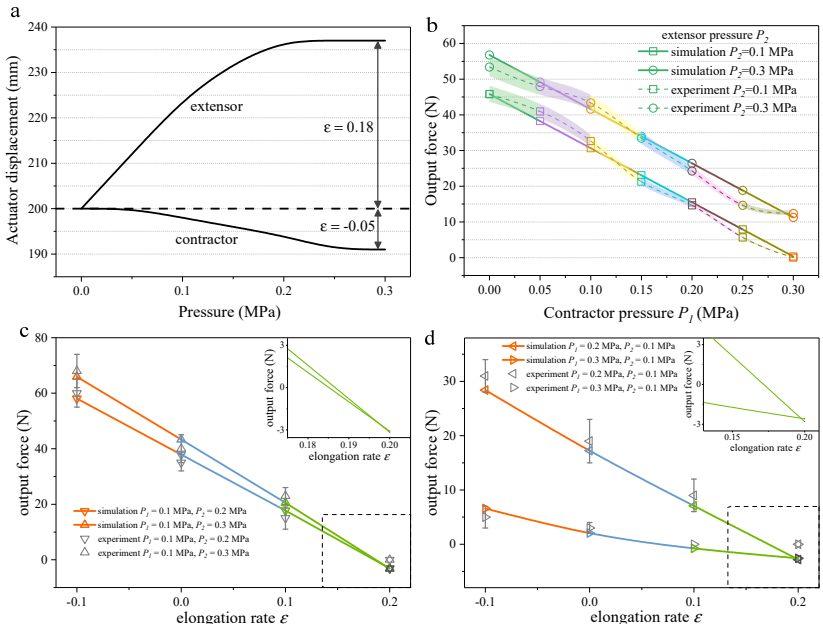

Figure 8. (**a**) The pressure-displacement result of independently pressurizing the extensor or contractor muscles of the actuator separately. (**b**) The pressure-force simulation and experiment results of pressurizing the extensor and contractor muscles of the actuator simultaneously. (**c**,**d**) When single contractor or extensor pressure is fixed and the other is varying, the elongation rate-output force simulation and experiment results.

The method of verifying the mathematical model of output force is to first pressurize the extensor muscle with air pressures of 0.1 MPa, 0.2 MPa, 0.3 MPa, and collect the output force corresponding to the air pressure by the load cell. Next, we start to continuously pressurize the contractor muscle, and the contractor will produce contraction force. This contraction force will gradually reduce the output force of the extensor. The elongation rate of the actuator can be controlled by adjusting the *z*-axis stepper motor of the three-degree-of-freedom platform, even under pressurized state. The test results and simulation results when elongation rate is zero are shown in Figure 8b. We find that the relationship between the input pressure and output force is nonlinear and hysteretic. The repeatability is also not so excellent. In fact, it reveals some general challenges that soft actuator are faced with, that is, high nonlinearity, serious hysteresis, and poor repeatability, which mainly influence the accuracy. We think the nonlinearity is mainly determined by nonlinear mechanics of the soft materials, such as hyperelasticity of the silica gel bladder and fabric layers.

When the pressure of the extensor muscle is 0.1 MPa, the required pressure of the contractor muscle is 0.3 MPa to balance the output force of the extensor. At this time, the soft actuator output force is zero, and the length is the initial length. After calculation, the average error between the test results and the simulation results is 7.36%. In the modeling process, we considered the friction between the fabric layer and the silicone body, but ignored the friction between the yarns of the fabric layer. Although it is small, it will also have a certain impact on the results. The second is that when the actuator is pressurized, although the bracket is fixed to limit its buckling, there are still some gaps in it, so a small amount of buckling occurs. These two factors are the main reasons for the error.

The elongation rate of the actuator can be controlled by adjusting the *z*-axis stepper motor of the three-degree-of-freedom platform, even under pressurized state. We simulated the output force results of changing the elongation rate when the pressure of the extensor and contractor muscles is fixed. As shown in Figure 8c, when the contracting muscle is fixed at 0.1 MPa and the extensor muscle is fixed at 0.2 and 0.3 MPa, respectively, the result of the actuator output force during the process of changing the elongation from −0.1 to 0.2. Similarly, Figure 8d shows the output force results when the extensor muscle is fixed at 0.1 MPa and the contracting muscle is fixed at 0.2 and 0.3 MPa, respectively. We can find that when the pressure is fixed, the output force of the actuator is inversely proportional to the elongation rate. At the same time, when the contractor muscle pressure is fixed, the greater the extensor muscle pressure, the more obvious the effect of elongation rate on the output force, and when the extensor muscle pressure is fixed, the greater the contractor muscle pressure, the weaker the effect of elongation rate. Because the output force of the two muscles is in the opposite direction, the elongation rate will increase or decrease the output force.

4.2. Static Stiffness Analysis

Since conventional pneumatic contractor or extensor actuators often have only one inflation chamber, they have a single fixed stiffness value at invariable length or input pressure. The reason is that the stiffness is a result of the pressure inside, and higher pressures result in greater stiffness. The ECFA proposed in this research has both extensor and contractor chambers. Under different pressures, they are pressurized into the two inflation chambers, which has the potential to change and control its stiffness.

Tensile stiffness experiments were performed. The ECFA was suspended vertically again, this time the distal end was free. The actuator was initially at its relaxed length of 200 mm. Next, a load was hanged on the distal end of the ECFA, resulting in corresponding axial displacements (Figure 9a). The stiffness can be calculated at unpressurized state by the gradient of the gravity/displacement. At pressurized state, the method is similar. We first tested the tensile stiffness of the extensor and contractor separately. Figure 9b shows the corresponding tensile stiffness of ECFA when pressurizing the contractor or extensor only. Such experimental results are foreseeable, that is, the tensile stiffness is constantly changing and increasing with pressurizing increasingly. With the increase of extensor pressure, the length of the actuator changes greatly, because the tensile resistance of the contractor

to the extensor is relatively small. However, the extensor has a great influence on the contractor, resulting in a small change in length when only the contractor is pressurized. The experimental results of the displacement and output force can be explained here. The extensor generates thrust force when pressurized, and when the contractor is pressurized with at least three times the extensor pressure, the thrust force can be offset. Under the same pressure, the stiffness of extensor is greater than that of contractor.

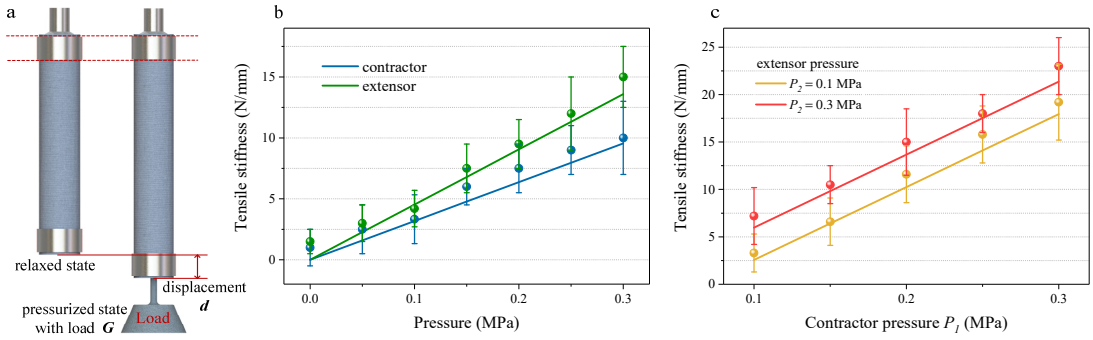

Figure 9. Tensile stiffness of the actuator. (**a**) Diagram of the method for testing the stiffness of the actuator. (**b**) The pressure-stiffness simulation and experiment result of independently pressurizing the extensor or contractor muscles of the actuator separately (scatter plots is the test results). (**c**) The actuator tensile stiffness simulation and experiment results of pressurizing the extensor and contractor muscles simultaneously (scatter plots is the test results).

The novelty of our research is that when the extensor and contractor muscles are pressurized simultaneously, how the actuator tensile stiffness changes. Similarly, firstly, we pressurized the extensor with 0.1 MPa, next pressurized the contractor with 0.1 MPa and 0.3 MPa respectively, and then suspended weights at the end of ECFA and recorded the axial displacement of this state. Sometimes the displacement is very small. We used a Vernier caliper to measure the average value repeatedly, which is the main reason for the error of experiments and simulation results. Then the extensor was pressurized with 0.3 MPa, and the above steps were repeated for measurement. Tensile stiffness can be determined from the gradient of the gravity/displacement (Figure 9c). It can be found that when the extensor pressure is fixed, increasing contractor pressure within a certain range will reduce the stiffness of the actuator, but according to the simulation trend, when the pressure is increased to a level, the stiffness will increase in the reverse direction. Compared with the stiffness of pressurizing only the extensor or contractor, it can be found that the actuator stiffness is increased, which shows that the antagonistic relationship between the extensor and contractor can indeed increase the stiffness. This can be proved that the tensile stiffness of the proposed actuator has significant variable stiffness capability compared with the traditional single chamber actuator. And compared with the previous variable stiffness soft actuator that can adjust stiffness in 0.036–0.096 N/mm with pressure 0.1–0.4 MPa [24], the proposed soft actuator in this paper has a larger tunable range of 2.5–26 N/mm with pressure 0–0.3 MPa.

The proposed actuator possesses not only variable stiffness, but controllable stiffness. The antagonism generated by redundant driving of ECFA is similar to the antagonism between two springs, as shown in Figure 10a, an object *G* keeps balance under the action of contraction spring ① and extension spring ②. F1 is the extension force produced by contraction spring ① and F2 is the contraction force produced by extension spring ②. When the object is given a left force ΔF, a small left displacement Δx will be generated. Stiffness k is defined as: k = ΔF/Δx. It can be seen from Figure 10b that at this time, the output extension force of spring ① increases, and the contraction force of spring ② increases. If only one side fixes a spring, the displacement will be larger and the stiffness will be shown smaller when the same ΔF is applied. Therefore, using two springs will increase the stiffness of the system, which is the same as the principle of the combination of extensor and contractor in this paper, that is, when the object has left displacement, the spring ① shortens and the output

extension force increases (this can be considered that the length of the contractor in ECFA shortens, the braid angle α increases, the Fcontractor decreases and output extension force increases); the spring ② lengthens and the output contraction force increases (it can be considered that the extensor in ECFA lengthens, the Fextensor is larger and the contraction force is larger). Therefore, it possesses not only variable tensile stiffness, but also variable compressive stiffness. However, the stiffness of the spring is variable but not controllable. The actuator proposed in this paper via two chamber pressures to control the overall stiffness of the actuator. When the external force ΔF acts on one end of the actuator to achieve balance: $F = \Delta P \cdot A$, where A is the effective area of the actuator. $k = \Delta P \cdot A/\Delta x$. Therefore, the displacement Δx can be measured by tools and ΔP can be adjusted by the system shown in Figure 6, which can realize the control of the stiffness.

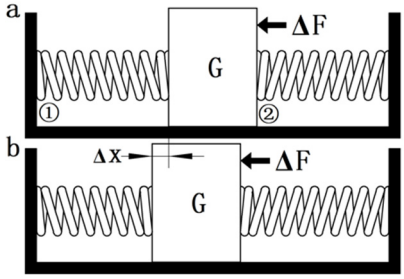

Figure 10. Compound springs model for analogy to actuator based on the antagonism principle. (**a**) The two springs are in a balanced state. (**b**) The external force causes two springs to elongate and contract respectively.

Specifically, the ECFA can perform variable stiffness under a fixed length. The ECFA is initially at its unpressurized nominal length of 200 mm, then the extensor is pressurized to 0.05 MPa, resulting in elongation relative to the nominal length. Then increasing the contractor pressure until the length of the ECFA is reduced to the nominal length again. The pressure of contractor needed for this purpose is 0.14 MPa. The stiffness at this time also can get from the gradient of gravity/displacement and it is found that the stiffness is 2 N/mm. In order to prove the possibility of obtaining different stiffness values at the same length, the extensor pressure was increased to 0.07 MPa. This again causes the ECFA to become longer than the nominal length, so the contractor pressure increases again until the nominal length is reached. The contractor pressure required for this purpose is 0.23 MPa. Again, the stiffness is found by experiment and calculated to be 10.5 N/mm. We also tested that when the extensor is 0.12MPa, the pressure of the corresponding contractor is 0.34 MPa, and the calculated stiffness is 20.3 N/mm. It can be seen that at the same length, the different stiffness can be achieved. In order to further verify that the stiffness of ECFA can be adjusted on the fixed length, we take the nominal length of 210 mm and 220 mm for the retest, and Table 3 summarizes the stiffness results of ECFA.

Table 3. Results of varying stiffness without length changing of the actuator.

Experiment No.	ECFA Length (mm)	Contractor P1 (MPa)	Extensor P2 (MPa)	Tensile Stiffness (N/mm)
1	200	0.14	0.05	2
2	200	0.23	0.07	10.5
3	200	0.34	0.12	20.3
4	210	0.15	0.08	5.67
5	210	0.22	0.1	12.5
6	210	0.32	0.15	21.2
7	220	0.16	0.1	7.5
8	220	0.22	0.15	13.6
9	220	0.28	0.2	18.67

Unlike some previous soft actuator, the new actuator proposed in this research has the following advantages in the aspect of variable stiffness. One is that when two chambers of the proposed actuator are pressurized, the stiffness will change significantly and be controlled conveniently compared with that of a single chamber pressurized. The other is that the stiffness of the proposed actuator can be adjusted without resulting in a change of actuator length.

It is important to study the tensile stiffness of soft actuator, but when applied in bending engineering, bending stiffness becomes indispensable. To this end, we tested the bending stiffness at the corresponding pressure. The three-point measurement method is used to obtain the bending stiffness value. Figure 11a shows that when the span of two supporting points is S, the weight is used to apply downward force to the actuator, resulting in the actuator bending downward and a vertical deformation D, so the bending stiffness can be obtained from the applied force/deformation.

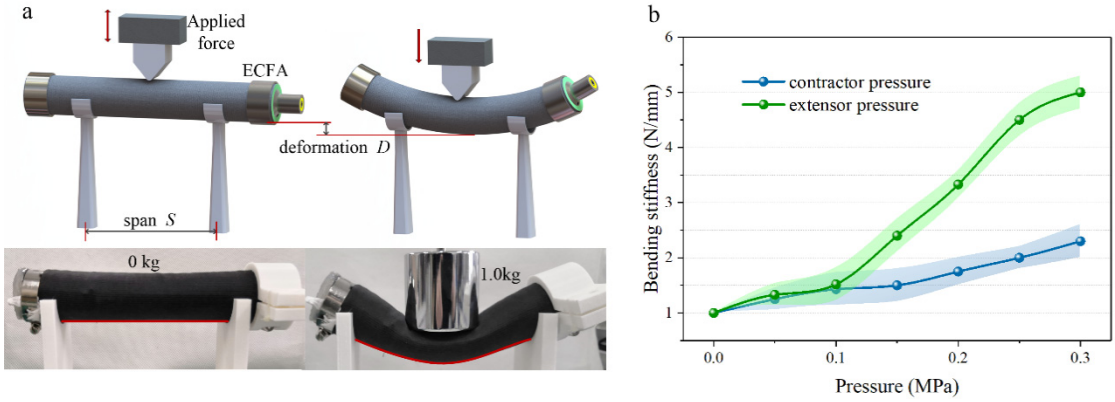

Figure 11. Bending stiffness of the actuator. (**a**) Stiffness estimation under flexural loading of the actuator. (**b**) The pressure-stiffness experiment result of independently pressurizing the extensor or contractor muscles of the actuator separately.

Similar to the test of tensile stiffness, we tested the bending stiffness of ECFA when only the extensor or contractor muscles were pressurized. The result of bending stiffness as shown in Figure 11b. The bending stiffness will enhance with the pressure increasingly, but the increase is not obvious compared with tensile stiffness. Similarly, under the same pressure, the bending stiffness of the extensor-only pressurized is greater than that of the contractor.

Based on the analysis of the tensile and bending stiffness of the actuator, we manufactured a soft mechanical manipulator with variable stiffness, which consists of two parallel soft actuators and four sets of cages. The cages are divided two symmetrical parts, which are tightened with lightweight bolts and nuts. The four tubes pressurize the four inflation chambers of the manipulator. When the pressure is applied to bend the soft manipulator, the bending angle is defined as α, as shown in Figure 12a. The method of testing the stiffness is to add weights to the free end of the soft manipulator when it bends, which will cause the free end to displace (Figure 12b). Similarly, the stiffness is obtained from the gradient between the force and displacement. Figure 9c–e shows our experimental process, in which one ECFA's extensor muscle is pressurized, and the other ECFA's contractor muscle is pressurized. A 0.5 kg weight is placed the free end in the bending state, the displacement can and corresponding stiffness be measured and calculated. We adjust the pressure of the four chambers to keep the soft manipulator in a fixed bending posture, and then test the stiffness under the corresponding pressure. The results are shown in Table 4.

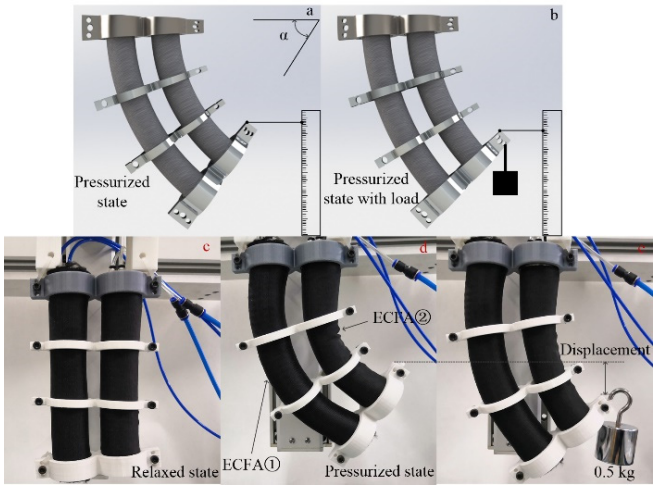

Figure 12. (**a**,**b**) are the method to test the stiffness of the soft manipulator, that is, applying weights to produce displacement under pressurized bending state. (**b–e**) are a period of experiment process when the manipulator under relaxed and pressurized state and (**c**) is bending attitude when the extensor of ECFA① is 0.2MPa and the contractor of ECFA② is 0.1 MPa.

Table 4. Results of varying stiffness without bending angle changing of the manipulator.

Experiment No.	Bending Angle (degree)	ECFA①		ECFA②		Stiffness (N/mm)
		Contractor (MPa)	Extensor (MPa)	Contractor (MPa)	Extensor (MPa)	
1	50°	0.05	0.32	0.3	0.02	1.67
2	50°	0.08	0.35	0.25	0.14	6.5
3	50°	0.15	0.38	0.2	0.24	12
4	40°	0.02	0.23	0.18	0.03	0.5
5	40°	0.12	0.26	0.15	0.08	4.6
6	40°	0.18	0.3	0.12	0.15	8.5
7	30°	0.03	0.1	0.08	0.02	0.25
8	30°	0.04	0.12	0.05	0.05	3.3
9	30°	0.07	0.18	0.03	0.12	5.2

The stiffness of the soft arm depends on the tensile and bending stiffness of ECFA. From the experimental results, it can be found that the stiffness of the arm is relatively small. The main reasons we believe are mainly two points: One is that the weights will cause the ECFA to deform irregularly. It can be seen from Figure 12e that the curvatures of the two ECFAs are significantly different from those in Figure 12d, which is attributed to the lower bending stiffness. The another is caused by the tension and compression stiffness of ECFA itself. As shown in Figure 12d, ECFA② itself has contraction force and ECFA① has extension force. After applying a weight, these two forces are enhanced. The torque caused by these two forces will increase the tendency to return to the initial state, which is attributed to the tensile stiffness of ECFA. The stiffness is mainly achieved by controlling the extensor and contractor muscles of the two actuator units. The tensile stiffness and bending stiffness of the actuator play a crucial role. To analyze separately, ECFA① has a certain tensile stiffness when the extensor muscle of ECFA① is pressurized and the contractor muscle of ECFA② is pressurized. Due to the coupling relationship between the two actuators, the soft arm will bend and have a certain bending stiffness. In short, for the soft arm, tensile stiffness and bending stiffness exist at the same time and influence each other.

5. Conclusions

In this study, we presented methods to exploit the mechanical anisotropy of elastic and woven fabrics to create fabric-based soft actuators based on the antagonistic mechanism of extensor and contractor muscles that can achieve varying stiffness. The soft actuators break through some of the

limitations of single chamber PAM as well as possessing additional features, that is, the actuator has bidirectional action allowing it to both extend and contract and create force in bidirectional.

Based on the principle of virtual work, a novel mathematical model has been developed for the actuator which describes its output force and static stiffness. The force model has been verified experimentally including pressure-force and elongation rate-force experiments respectively, the average error between the mathematical model and the experimental results being less than 10%. Moreover, static stiffness is the derivative of output force to displacement and the stiffness of an actuator is dependent on the input pressure. The influence of only pressurizing the extensor or contractor muscles on the stiffness of the actuator were simulated and tested separately, and the average errors were less than 10%. However, the length of traditional pneumatic soft actuators is a function of pressure, which means that it is impossible to vary stiffness of the actuator without varying its length. We have demonstrated that the proposed actuator based on antagonistic mechanism can adjust its stiffness without changing in length and many length-stiffness experiments were conducted to explore its varying stiffness capability that independent of position. In addition, the influence of only pressurizing extensor or contractor muscles on the bending stiffness of the actuator was tested, because we manufactured a soft mechanical manipulator with variable stiffness using the new actuators. The manipulator's stiffness depends on the tensile and bending stiffness of the actuator, and the manipulator can vary in stiffness under a fixed bending attitude, so we conducted numerous experiments to verify it.

In the future, the mathematical model will be further improved by considering other dynamic forces, such as the inertial force generated by instantaneous pressure, to enhance the mathematical model and reduce the average percentage error. We will also try to improve the structure of the soft manipulator to increase its stiffness and better adapt to actual projects.

Author Contributions: Conceptualization, Y.C. and J.Z.; methodology, Y.C. and J.Z.; software, Y.C. and J.Z.; validation, Y.C. and J.Z.; formal analysis, Y.C.; investigation, J.Z.; resources, Y.C.; data curation, Y.C.; writing—original draft preparation, Y.C. and J.Z.; writing—review and editing, Y.G.; visualization, Y.C. and J.Z.; supervision, Y.G.; project administration, Y.G.; funding acquisition, Y.C. All authors have read and agreed to the published version of the manuscript.

Funding: This research was funded by National Natural Science Foundation of China (NSFC) under Grant 51905067, U1908228, in part by High-Tech Ship Project of Ministry of Industry and Information Technology (MIIT) under Grant 2018ZX04001-021, and in part by Fundamental Research Funds for the Central Universities under Grant 3132020115.

Acknowledgments: The authors thank the reviewers for their elaborate and incisive suggestions.

Conflicts of Interest: The authors declare no conflict of interest.

References

1. Tadano, K.; Akai, M.; Kadota, K.; Kawashima, K. Development of grip amplified glove using bi-articular mechanism with pneumatic artificial rubber muscle. In Proceedings of the IEEE International Conference on Robotics & Automation IEEE, Anchorage, AK, USA, 3–7 May 2010.
2. Wang, Y.K.; Guo, C.; Li, J.; Wang, Z.L. Design of a Flexible Bending Biomimetic Octopus Arm Unit with Embedded SMA Wires. *Appl. Mech. Mater.* **2010**, *44*, 2543–2547. [CrossRef]
3. Chiba, S.; Waki, M.; Wada, T.; Hirakawa, Y.; Masuda, K.; Ikoma, T. Consistent ocean wave energy harvesting using electroactive polymer (dielectric elastomer) artificial muscle generators. *Appl. Energy* **2013**, *104*, 497–502. [CrossRef]
4. Ansari, Y.; Manti, M.; Falotico, E.; Mollard, Y.; Cianchetti, M.; Laschi, C. Towards the development of a soft manipulator as an assistive robot for personal care of elderly people. *Int. J. Adv. Robot. Syst.* **2017**, *14*, 1–17. [CrossRef]
5. Manti, M.; Thuruthel, T.G.; Falotico, F.P.; Pratesi, A.; Falotico, E.; Cianchetti, M.; Laschi, C. Exploiting morphology of a soft manipulator for assistive tasks. In Proceedings of the Conference on Biomimetic and Biohybrid Systems, Stanford, CA, USA, 25–28 July 2017; Springer: Cham, Switzerland, 2017; pp. 291–301.
6. Kim, Y.J.; Cheng, S.; Kim, S.; Iagnemma, K. A novel layer jamming mechanism with tunable stiffness capability for minimally invasive surgery. *IEEE Trans. Robot.* **2013**, *29*, 1031–1042. [CrossRef]

7. Ranzani, T.; Gerboni, G.; Cianchetti, M.; Menciassi, A. A bioinspired soft manipulator for minimally invasive surgery. *Bioinspir. Biomim.* **2015**, *10*, 035008. [CrossRef] [PubMed]
8. Olaru, R.; Salceanu, A.; Calarasu, D.; Cotae, C. Magnetic fluid actuator. *Sens. Actuators A* **2000**, *81*, 290–293. [CrossRef]
9. Manti, M.; Pratesi, A.; Falotico, E.; Cianchetti, M.; Laschi, C. Soft assistive robot for personal care of elderly people. In Proceedings of the IEEE International Conference on Biomedical Robotics and Bio-mechatronics, Singapore, 26–29 June 2016; pp. 833–838.
10. Yi, J.; Chen, X.; Song, C.; Wang, Z. Fiber Reinforced Origamic Robotic Actuator. *Soft Robot.* **2018**, *5*, 81–92. [CrossRef] [PubMed]
11. Najmuddin, W.S.W.A.; Mustaffa, M.T. A study on contraction of pneumatic artificial muscle (PAM) for loadlifting. *J. Phys. Conf. Ser.* **2017**, *908*, 012036. [CrossRef]
12. Al-Ibadi, A.; Nefti-Meziani, S.; Davis, S. Novel models for the extension pneumatic muscle actuator performances. In Proceedings of the 2017 23rd International Conference on Automation and Computing (ICAC), Huddersfield, UK, 7–8 September 2017.
13. Chen, Y.; Zhang, J.; Gong, Y. Utilizing Anisotropic Fabrics Composites for High-Strength Soft Manipulator Integrating Soft Gripper. *IEEE Access* **2019**, *7*, 127416–127426. [CrossRef]
14. Xiang, C.; Giannaccini, M.E.; Theodoridis, T.; Hao, L.; Nefti-Meziani, S.; Davis, S. Variable stiffness Mckibben muscles with hydraulic and pneumatic operating modes. *Adv. Robot.* **2016**, *30*, 889–899. [CrossRef]
15. Tanaka, D.; Kamo, D.; Maehara, M.; Nakamura, T. Development of two types of 2DOF wrist joint driven by pneumatic artificial muscles. In Proceedings of the 2013 IEEE International Conference on Mechatronics (ICM), Vicenza, Italy, 27 February–1 March 2013.
16. Belforte, G.; Eula, G.; Ivanov, A.; Sirolli, S. Soft Pneumatic Actuators for Rehabilitation. *Actuators* **2014**, *3*, 84–106. [CrossRef]
17. Ferraresi, C.; Franco, W.; Quaglia, G. Bi-Directional flexible Pneumatic Actuator. In Proceedings of the Fift Internazional Symposium on Fluid Power JFPS 2002, Nara, Japan, 12–15 November 2002; pp. 25–30.
18. Jeong, H.; Kim, J. Echinoderm Inspired Variable Stiffness Soft Actuator with Connected Ossicle Structure. In Proceedings of the 2019 International Conference on Robotics and Automation (ICRA) 2019, Montreal, QC, Canada, 20–24 May 2019.
19. Bishop-Moser, J.; Krishnan, G.; Kota, S. Force and Hydraulic Displacement Amplification of Fiber Reinforced Soft Actuators. In Proceedings of the ASME International Design Engineering Technical Conferences & Computers & Information in Engineering Conference, Portland, OR, USA, 4–7 August 2013.
20. Sheppard, D.; Xiao, P.; Chemelewski, W.; Johnson, D.D.; Henkelman, G. A generalized solidstate nudged elastic band method. *J. Chem. Phys.* **2012**, *136*, 074103. [CrossRef] [PubMed]
21. Chou, C.P.; Hannaford, B. Measurement and modeling of McKibben pneumatic artificial muscles. *IEEE Trans Robot Automat.* **1996**, *12*, 90102.
22. Zang, K.; Wang, Y.; Fu, X.; Hu, X. Study on Modeling of Mckibben Pneumatic Artificial Muscle. In Proceedings of the 2008 International Conference on Intelligent Computation Technology and Automation, Hunan, China, 20–22 October 2008.
23. Al-Fahaam, H.; Nefti-Meziani, S.; Theodoridis, T.; Davis, S. The design and mathematical model of a novel variable stiffness extensorcontractor pneumatic artificial muscle. *Soft Robot.* **2018**, *5*, 576–591. [CrossRef] [PubMed]
24. Fei, Y.; Wang, J.; Pang, W. Novel Fabric Based Versatile and StiffnessTunable Soft Gripper Integrating Soft Pneumatic Fingers and Wrist. *Soft Robot.* **2019**, *6*, 1–20. [CrossRef] [PubMed]